Interference effects in the autoionization of 4F7H and 6DNI states of Barium

van Leeuwen, R.; Ubachs, W.M.G.; Hogervorst, W.; Aymar, M.; Luckoenig, E.

published in
Physical Review A. Atomic, Molecular and Optical Physics
1995

DOI (link to publisher)
10.1103/PhysRevA.52.4567

document version
Publisher's PDF, also known as Version of record

Interference effects in the autoionization of $4f7h$ and $6dni$ states of barium

R. van Leeuwen, W. Ubachs, and W. Hogervorst
Laser Centre Vrije Universiteit, Department of Physics and Astronomy, De Boelelaan 1081, 1081 HV Amsterdam, The Netherlands

M. Aymar and E. Luc-Koenig
Laboratoire Aimé Cotton, Centre National de la Recherche Scientifique II, Bâtiment 505, 91405 Orsay Cedex, France*
(Received 17 March 1995)

In a two-step pulsed laser experiment $4f_{5/2}7h$ $J=4,5,6$, autoionizing levels of Ba were excited. The $4f_{5/2}7h$ levels interact with $6d_{5/2}ni$ levels resulting in complex interference patterns. The excitation spectra were calculated using the eigenchannel R-matrix method in combination with multichannel quantum-defect theory. These R-matrix calculations reproduce the excitation spectra, including the interference patterns which involve q-reversal and stabilization against autoionization in the $6d_{5/2}ni$ series, very well. The excitation spectra for $J=5$ are also analyzed using a phase-shifted R-matrix model in which only three channels had to be included to reproduce the main experimental features. The three-channel model clearly shows that the stabilization against autoionization in the $6d_{5/2}ni$ Rydberg series is a result of interference in the decay of $4f_{5/2}7h$ and $6d_{5/2}ni$ levels, autoionizing into the same $6d_{3/2}\epsilon i$ continuum.

PACS number(s): 32.80.Dz, 32.80.Fb, 31.50.+w

I. INTRODUCTION

In recent years much attention has been given to high-lying autoionizing states of alkaline-earth-metal atoms. In multistep laser experiments series of doubly excited states were studied at increasingly high energy [1–3]. Simultaneously considerable progress in the capability of calculating photoionization cross sections of the alkaline-earth-metal atoms has been achieved. In particular the combination of eigenchannel R-matrix calculations and multichannel quantum-defect theory (MQDT) [4–6] has been successful in reproducing experimental photoionization spectra, at excitation energies up to 7 eV above the first ionization limit for Ba [7–9].

In alkaline-earth-metal atoms the two valence electrons move in the field of a doubly charged core. The valence electrons of the heavier alkaline-earth metals are only loosely bound, facilitating the study of electron correlation effects using laser spectroscopic techniques. However, the spatial extension of the 2^+ core complicates the interpretation of correlation effects. Therefore much experimental effort has recently gone into reducing core penetration effects by exciting both valence electrons to states with high orbital angular momentum l [10,11]. Since the $^1S_0$ ground state of alkaline-earth-metal atoms contains two ns electrons (with $n=5$ for Sr and $n=6$ for Ba) this requires multistep laser excitation. To reach a high-l value for one of the electrons the Stark switching technique [12] can be applied, in which excitation of the first electron takes place in an electric field, followed by sequential laser excitation of the inner electron. Examples of this technique are the excitation of $6gnl$ states in Sr by Eichmann, Lange, and Sandner [13] and $8snl$ states of Ba by Camus *et al.* [14].

In the present experiment we use metastable states of the $5d^2$ configuration and weak configuration mixing to populate high-lying doubly excited levels of barium with a fairly high l for both electrons. In a resonant two-step pulsed laser experiment based on an isolated-core-excitation scheme (ICE) [15] $4f7h$ $J=4-6$ autoionizing states of barium, lying in the energy range between the $6d_{3/2}$ and $6d_{5/2}$ thresholds at 5.7 eV above the $6s$ ionization limit were excited via $5d7h$ intermediate levels.

The ICE experimental technique has been shown to be adequate to excite Ba $4fnl$ autoionizing levels from $5dnl$ levels [10,11] in spite of the collapse effect which affects the $4f$ orbital [16,17].

Complex interference patterns, resulting from the interaction between broad $4f_{5/2}7h$ resonances and narrow $6d_{5/2}ni$ series, were observed. The problem of Rydberg series of autoionizing states interacting with a broad resonance has been discussed in several papers [18–24]. In particular q reversal [25] across a contour of the broad resonance was first observed by Connerade [22] in Tl. In the energy range just above the first ionization limit it has been shown that interference between different autoionization decay channels of doubly excited states can lead to an important narrowing of linewidths and even to stabilization against autoionization [18,19].

Data on doubly excited states are often analyzed using empirical MQDT models. From these models no detailed information on the wave functions of excited levels can be deduced. This information, which is of importance when levels are considered for further excitation to double Rydberg states, may be obtained from eigenchannel R-matrix calculations such as recently performed on various autoionizing Rydberg series of Ba [8,9,26]. Here the results of an experimental study of interacting $4f_{5/2}7h$ and $6d_{5/2}ni$ states in the 87 970–88 110-cm^{-1} range are confronted with eigenchannel R-matrix calculations. The one-step excitation spectra of $5d_{3/2}7h$ levels were investigated in detail, both theoretically and experimentally, in order to determine the correct wave functions for these intermediate levels. Next the excitation

*The Laboratoire Aimé Cotton is associated with the Université Paris-Sud, Paris, France.

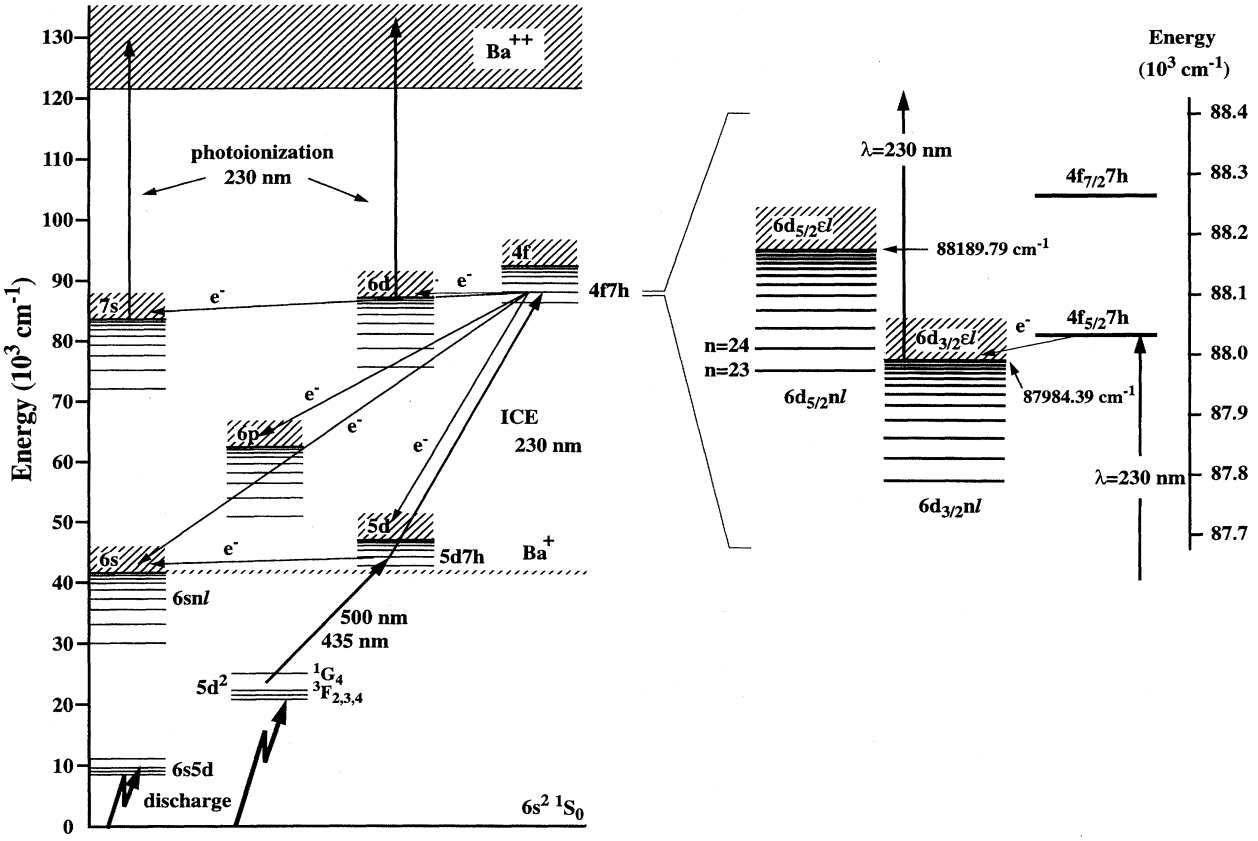

FIG. 1. Energy-level diagram of barium for the two-step laser excitation of $4f_{5/2}7h$ $J'=4-6$ levels via autoionizing intermediate $5d_{3/2}7h$ $J=5$ levels and starting out from metastable $5d^2J=4$ levels. The arrows indicating autoionization paths are denoted by e^-. Only the highly excited $6d_{3/2}$ and $7s$ ions, produced in the autoionization process of the $4f_{5/2}7h$ levels, may be excited by the UV laser to yield Ba^{2+} signal; this is indicated by vertical arrows. The right-hand side of the figure reveals more details in the energy range in which the $4f_{5/2}7h$ levels are located.

spectra of the even parity $4f7h$, $6dni$ $J=4-6$ levels were investigated. An excellent quantitative agreement between calculated and observed excitation spectra was found, providing correct assignments for all observed features. The phase-shifted MQDT formalism [20,27,28] is used to analyze the observed interference pattern for $J=5$. A simplified treatment, involving only three channels, is developed to explain the interference, q reversal, and stabilization effects in the autoionization process.

II. EXPERIMENT

The $4f_{5/2}7h$ $J'=4-6$ autoionizing states of barium were studied in a resonant two-step pulsed laser experiment, based on an isolated-core-excitation scheme and using an atomic beam. The excitation scheme showing the relevant energy levels and ionization limits is shown in Fig. 1. First, Ba atoms in metastable $5d^2\ ^3F_4$ or $^1G_4$ states were excited to an autoionizing intermediate $5d_{3/2}7h$ $J=5$ state with a tunable pulsed dye laser (bandwidth 0.07 cm^{-1}). This dye laser, operating on Coumarine dyes, was pumped by 30% of the third harmonic output (355 nm) of a Nd:YAG (yttrium aluminum garnet) laser. The intermediate $5d7h$ states, located just above the first $6s$ ionization limit, can be excited from $5d^2$ levels because of the mixing of the $5dnf$ and $5dnh$ wave functions. An experimental spectrum of the one-step laser excitation from the $5d^2\ ^1G_4$ level, recorded by Ba^+ detection, is shown in Fig. 2. The $5dnh$ states are identified in jK coupling. In the second step, the frequency-doubled output of a second dye laser, pumped by the remaining 70% of the 355-nm output of the YAG laser, further excited the Ba atoms from an intermediate $5d_{3/2}7h[K]$ $J=5$ state to $4f_{5/2}7h$ J' states. For this purpose about 1 mJ/pulse of UV light was produced in a β-BaB_2O_4 (BBO) crystal at wavelengths close to the $Ba^+5d_{3/2}\rightarrow 4f_{5/2}$ ionic transition at 230.5 nm.

For the high-lying $4f_{5/2}7h$ states at 5.7 eV above the $6s$ ionization limit many continua are available for autoionizing decay. The Coulomb repulsion between the two valence electrons couples the $4f_{5/2}7h$ states to several continua, resulting in Ba^+ ions in $6s$, $5d_j$, $6p_j$, $7s$, and $6d_j$ states and electrons in a wide range of energies. As can be seen from Fig. 1 the $4f_{5/2}7h$ states are located in between the upper and lower $6d_j$-ionization limit (at 88 189.79 cm^{-1} for $j=5/2$ and 87 984.39 cm^{-1} for $j=3/2$). The $4f_{5/2}7h$ states interact with $6d_{3/2}\epsilon l'$ continuum states ($l'=4$ or 6) via dipole coupling. Autoionization of the $4f_{5/2}7h$ states is therefore expected to

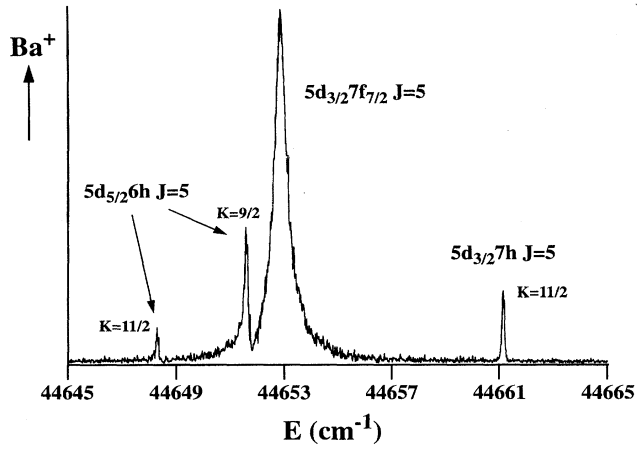

FIG. 2. Experimental spectrum of $5dnh$ levels in the vicinity of the strong $5d_{3/2}7f$ $J=5$ resonance. The $5dnh$ components are excited because of a small amount of $5dnf$ $J=5$ character in their wave functions. The recorded Ba^+ signal is shown vs the energy with respect to the $6s^2\ ^1S_0$ ground state. The $5d_{3/2}7h$ $J=5$ state is used as an intermediate state for further excitation to $4f_{5/2}7h$ J levels.

result mainly in very slow electrons of a few meV energy and Ba^+ ions in the $6d_{3/2}$ state. Direct photoionization of ground-state Ba atoms by UV light as well as autoionization of the low-lying intermediate $5d_{3/2}7h$ level also creates slow electrons (0.17 and 0.33 eV, respectively). Since the energy resolution in our setup was not sufficient to distinguish between these different processes, electron detection was not feasible to record $4f7h$ spectra. Therefore, we resorted to Ba^{2+} detection. The ions in highly excited $6d_{3/2}$ (or $7s_{1/2}$) states, resulting from the autoionization process of the $4f_{5/2}7h$ states, were photoionized by the UV light. So at each wavelength the recorded Ba^{2+} signal is a product of the cross section for the excitation of the $4f_{5/2}7h$ resonances, the partial autoionization rate of the $4f_{5/2}7h$ states into $6d_{3/2}\epsilon l'$ (or $7s_{1/2}\epsilon l'$) continua and the photoionization cross section for the $6d_{3/2}$ (or $7s_{1/2}$) Ba^+ ions.

An important characteristic of Ba^{2+} detection is that atoms autoionizing into $6s\epsilon l'$, $5d_j\epsilon l'$, and $6p_j\epsilon l'$ continua are not detected since the energy of the UV photons is not sufficient for photoionization of ions in these states. Another characteristic of this detection method is that metastable $5d_{3/2}$ ions, produced by direct photoionization of Ba atoms in metastable states, can be excited to $4f_{5/2}$ states and subsequently photoionized by the UV laser, giving rise to a large Ba^{2+} signal at the $Ba^+ 5d_{3/2}\rightarrow 4f_{5/2}$ ionic transition energy. This ion transition, which appeared as a strong feature in the spectrum of the doubly excited $4f_{5/2}7h$ states, was used as a frequency marker.

The two counterpropagating dye laser beams with linear, crossed polarizations were aligned to overlap and perpendicularly intersect an atomic beam. Since the lifetime of the intermediate $5d7h$ state (≈ 100 ps) is short compared to the laser pulse duration (4–5 ns), the laser pulses were also temporally overlapped in the interaction region. The temporal overlap of the laser pulses turned out to be a sensitive parameter in the experiment. A small time delay of the UV-laser pulse strongly reduced the Ba^{2+} signal due to the fast autoionization of the intermediate state, while a small time delay of the laser pulse exciting the $5d7h$ state resulted in depletion of the initial $5d^2$ state due to direct photoionization of this state by the UV light.

The atomic beam was produced by radiatively heating a small tantalum oven containing a sample of natural barium. The Ba atoms were transferred to metastable $5d^2$ states in a low voltage discharge running at 800 mA between oven and filament with an estimated efficiency of 10^{-4}. The metastable barium atoms were excited between two capacitor plates both at zero potential. A few hundred ns after the laser excitation a pulse of 300 V was applied to one of the plates yielding a high collection efficiency for the ions. A grid at negative dc voltage, positioned in between this plate and the detector, was used to narrow down the velocity distribution of the ions, i.e., the width of the ion signals, to about 100 ns. The ions were detected with an electron multiplier. Direct photoionization by the UV light of Ba atoms in $6s5d$ metastable states, also populated in the discharge, gave rise to a strong Ba^+ signal. The Ba^+ and Ba^{2+} ion signals are separated by a μs in time due to the different time of flights of the ions. The Ba^{2+} signal was found in between Ca^+ and Sr^+ signals caused by photoionization of Ca and Sr impurities in the Ba sample. The 300-ns delay between the Sr^+ and Ba^{2+} signals was sufficient to separate the ion signals. The Ba^{2+} signals were integrated using a gated boxcar and stored on a computer.

The wavelengths of the visible output of the dye lasers were calibrated with an accuracy of 0.10 cm^{-1} using a home-built echelle-grating wavelength meter. The frequency-doubled output of the second dye laser was scanned across $4f7h$ resonances with a step size chosen equal to the instrumental linewidth of ≈ 0.2 cm^{-1}. At each wavelength setting the signal of 15 laser shots was summed. A compromise between step size and signal averaging had to be found since the discharge, running between oven and filament, could only be sustained for about 3 h for each oven filling. During this time production of metastable atoms slowly went down. To account for this decrease the Ba^{2+} signal was divided by the Ba^+ signal. This procedure also compensates for short term fluctuations in the metastable production and in the laser power, and as a result the signal-to-noise ratio is significantly increased.

A spectrum of $4f_{5/2}7h$ states excited from the $5d_{3/2}7h[11/2]$ $J=5$ state is shown in Fig. 3(a). A rapid oscillation on top of a broad structure with a full-width at half maximum (FWHM) of 45 cm^{-1} is observed. The broad resonance, centered at 88 033 (1) cm^{-1} above the $6s^2\ ^1S_0$ ground state, is identified as a $4f_{5/2}7h$ $J'=5$ state [8]. Since the $4f_{5/2}7h$ and $5d_{3/2}7h$ states have similar small quantum defects, the Ba^+ $5d_{3/2}\rightarrow 4f_{5/2}$ ionic transition is observed near to the center of the broad $4f7h$ resonance. The narrow resonances are identified as members of a $6dni$ Rydberg series converging to the $6d_{5/2}$ ionization limit (see Sec. IV). The $6d_{5/2}ni$ states show a remarkable stabilization against autoionization toward lower energies. The $n=23$ and 24 resonances have experimental linewidths close to the instrumental width of 0.2 cm^{-1}.

In Fig. 4(a) a spectrum of the excitation from the state

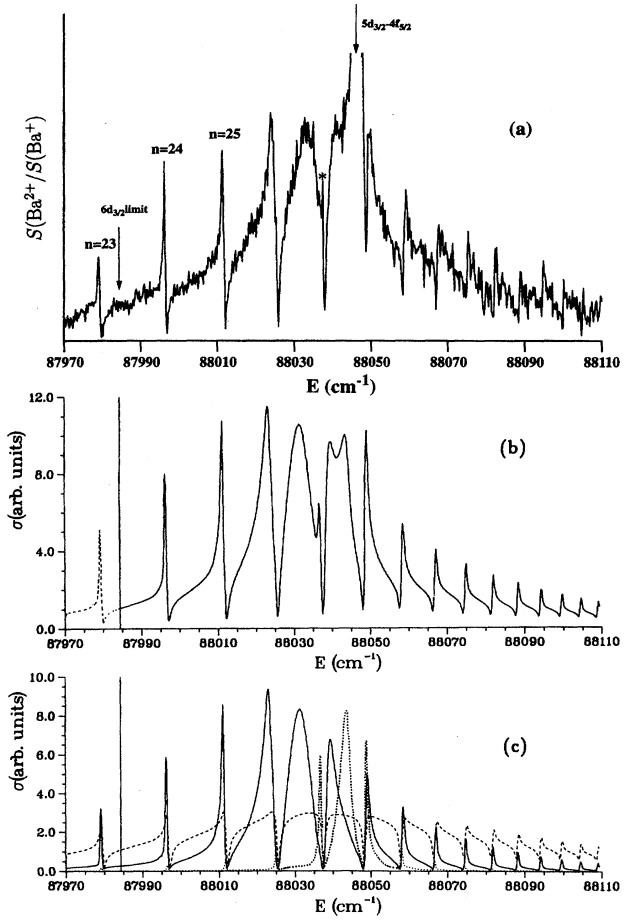

FIG. 3. Excitation spectra of $4f_{5/2}7h\ J'$ levels from the metastable $5d^2\ ^1G_4$ level via the $5d_{3/2}7h[11/2]\ J=5$ level, followed by photoionization of $Ba^+\ 6d_{3/2}$ and $7s$ ions. The energy scale is relative to the $6s^2\ ^1S_0$ ground state. (a) Experimental spectrum; the Ba^{2+} signal is divided by the Ba^+ signal to account for instabilities in the production of metastables and laser power fluctuations. The narrow resonances were identified as $6d_{5/2}ni$ levels. The $6d_{5/2}27i$ $J'=4$ at 88 037 cm^{-1} is denoted by (*). (b) Theoretical spectrum calculated with the eigenchannel R-matrix method. (c) The relative contributions of each final J' value to the theoretical spectrum in (b); dotted line, $J'=4$; full line, $J'=5$; dashed line $J'=6$.

$5d_{3/2}7h[9/2]\ J=5$ is shown. Again a complex interference pattern is observed, to be discussed in Sec. IV. The sharp feature at 88 036.8 cm^{-1}, identified as the $6d_{5/2}27i\ J'=5$ level (see Sec. IV), and the narrow $6d_{5/2}23i$ level show instrumental linewidth.

III. THEORETICAL PROCEDURE

Calculations concern the energy positions and wave functions of odd-parity $5dnh\ J=4,5$ levels, the excitation spectra of these levels from the $5d^2\ ^1G_4$ and $^3F_4$ levels and the excitation spectra of even-parity $J'=4-6$ levels located in the 87 970–88 110-cm^{-1} energy range (i.e., just below the $Ba^+\ 6d_{3/2}$ threshold and in between the $Ba^+\ 6d_{3/2}$ and $Ba^+\ 6d_{5/2}$ thresholds) from the jK-coupled $5d_{3/2}7h[11/2]$ and $5d_{3/2}7h[9/2]\ J=5$ levels. The theoretical approach, in

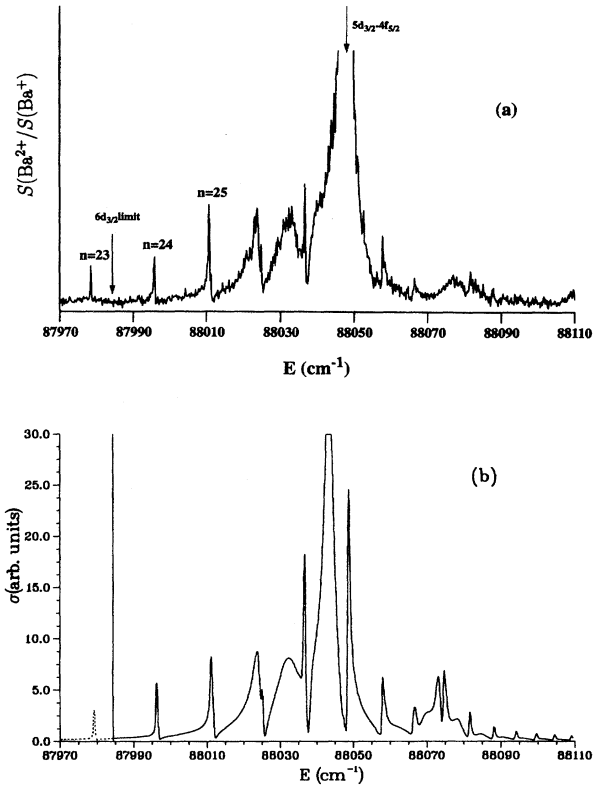

FIG. 4. (a) Experimental spectrum of the excitation of $4f_{5/2}7h\ J'$ levels from the metastable $5d^2\ ^3F_4$ level via the $5d_{3/2}7h[9/2]\ J=5$ level, followed by photoionization of Ba^+ $6d_{3/2}$ and $7s$ ions. (b) Theoretical spectrum calculated with the eigenchannel R-matrix method. The energy scale is relative to the $6s^2\ ^1S_0$ ground state.

which the eigenchannel R-matrix calculation and MQDT are combined, is described in detail in several publications [4–6,8,9,26] and only a brief outline is given here.

A. Eigenchannel R-matrix calculation

For a given J value the wave functions describing the pair of electrons outside a frozen Ba^{2+} core are determined variationally within a finite reaction volume using the jj-coupled R-matrix method. It explicitly includes the spin-orbit terms within the reaction volume, a sphere of radius r_0. Assuming that only one electron can escape from the reaction volume, the variational calculation gives the logarithmic derivatives of the wave functions at the surface of this reaction volume at selected energies E. Beyond r_0, the escaping electron is assumed to move in a pure Coulomb potential, longer-range multipole effects being neglected there. These effects play an important role for levels involving high-l orbital momenta [7]. It was shown recently [8] that a reaction volume of radius $r_0=50$ a.u. is necessary to describe $6dni$ and $7sni$ levels involving an $l=6$ orbital momentum for the outer electron correctly, and therefore this valid is used in the present calculations.

Several jj-coupled eigenchannel R-matrix calculations [26,29,30] have demonstrated the validity of this approach

for $4fnl$ levels which involve a $4f$ orbital which is extremely sensitive to centrifugal barrier effects [16,17].

The two-electron basis functions introduced in the variational calculation describe not only the open and weakly closed channels in which the outermost electron can escape from the reaction volume but also "strongly closed" channels where both electrons are confined within the reaction volume. These channels describe various polarization and correlation effects and play a decisive role in the success of eigenchannel R-matrix calculations.

The R-matrix calculations give the energy-dependent jj-coupled short-range reaction matrix $K(E)$ characterizing the interactions between the MQDT fragmentation channels for a given J symmetry. The dimension of the reaction matrix $K(E)$ equals the number of open or weakly closed fragmentation channels i ($i=\{nljn'l'j'\}$) in which one electron can escape from the R-matrix reaction volume.

The R-matrix calculation performed for the odd-parity $J=4$ ($J=5$) symmetry includes nine (11) open or weakly closed channels converging to the Ba^+ $6s$ and $5d_j$ thresholds. The description of the even-parity $J'=4-6$ symmetries in the energy range containing the Ba^+ $6d_j$ thresholds requires the determination of larger reaction matrices of dimensions 47, 44, and 37 for $J'=4$, 5, and 6, respectively. The R-matrix and MQDT calculations then include open and weakly closed $nljn'l'j'$ channels converging to the Ba^+, $6s$, $5d_j$, $6p_j$, $7s$, $6d_j$, $4f_j$, and $7p_j$ thresholds. Except for channels converging to the $4f_j$ and $7p_j$ thresholds, all possible l' values are used. For $4fn'l'$ and $7pn'l'$ channels, values are restricted to $l'\leq 5$. The set of channels for $J'=6$ is identical to that previously used to study $6dng$ $J=6$ levels [8] while those relevant to $J'=4$ or 5 differ from those used for calculating the $7sng$ $J=4$ [9] or $4fnf$ $J=5$ levels [26] only by the additional inclusion of $4fn'h$ channels. The variational basis sets used in this work include 1900–2500 two-electron functions depending on the symmetry.

B. MQDT treatment

Once the energy-dependent short-range reaction matrices $K(E)$ are determined, MQDT is used to extend the wave functions to distances larger than the R-matrix reaction volume. The eigenchannel MQDT formulation [31,32] or the phase-shifted MQDT formulation [20,27,28] is used to impose boundary conditions at large r and to calculate observables. As specific procedures were described in the papers quoted above, only some relevant details and formulas are given here.

1. Physical solutions and density of states in closed channels

Some basic formulas used in the eigenchannel MQDT formulation are briefly summarized. In the autoionizating energy range, the number of physical solutions equals the number N_0 of open channels. The asymptotic form of the collision eigenchannel function $\Psi_\rho(E)$, associated with an eigenphase shift $\pi\tau_\rho$ and satisfying standing-wave boundary conditions, is given by

$$\Psi_\rho(E)=\sum_{i'\in o}\Phi_{i'}[f_{i'}(r)\cos(\pi\tau_\rho)-g_{i'}(r)\sin(\pi\tau_\rho)] \times T_{i'\rho}(E)+\sum_{i\in c}\Phi_i P_i(\nu_i,r)Z_{i\rho}(E). \quad (1)$$

In Eq. (1), Φ represents a channel function associated with either an open ($i'\in o$) or a closed ($i\in c$) fragmentation channel, $f_{i'}$ and $g_{i'}$ are regular and irregular energy-normalized Coulomb functions, $P_i(\nu_i,r)$ is an exponentially decreasing Coulomb function [32] and ν_i is the effective quantum number in channel i. The coefficients $T_{i'\rho}(E)$ and $Z_{i\rho}(E)$ describe the relative admixture of the open and closed fragmentation channels, respectively.

The $4f_{5/2}7h$ levels, located between the Ba^+ $6d_{3/2}$ and $6d_{5/2}$ ionization limits, give rise to intricate structures corresponding to complex resonance patterns [21] because the $4f_{5/2}7h$ levels interact with dense Rydberg series of nonoverlapping resonances converging to the $6d_{5/2}$ ionization limit. Quantitative information on the positions and widths of the autoionizing levels, derived in a way that does not depend on the excitation scheme may be of great help to identify observed complex resonances. This information can be obtained [8,9,26] by analyzing the energy dependence of the partial densities of states in closed channels. Closed channels are better described in jK coupling, so jK-coupled closed channels $\bar{i}=\{nljn'l'[K]J'\}$ are introduced. The partial density of states in channel $\bar{i}$ is given by

$$ds_{\bar{i}}(E)=\sum_\rho [Z_{i\rho}(E)]^2. \quad (2)$$

Treating the $6d_{5/2}n'l'$ channels as open channels in the MQDT calculation of the density-of-states profiles or of the photoionization spectra results in the positions and "unperturbed widths" of the $4f_{5/2}7h[K]J'$ levels. These "unperturbed widths" correspond roughly to the spectral energy ranges over which the $6d_{5/2}n'l'$ series are perturbed by the $4f_{5/2}7h[K]J'$ levels.

2. Photoionization spectra

To calculate the photoionization cross-sections involved in the two steps of the excitation process, two different approximations are used.

(i) For the first step, the excitation spectra of odd-parity $5dnh$ $J=4,5$ levels from the $5d^2$ $^3F_4$ and $^1G_4$ levels are calculated by assuming that the $5d^2$ levels are contained within the R-matrix reaction volume. The wave functions of the initial states, accounting for configuration interaction, as well as the dipole matrix elements connecting the initial levels to the open and closed channels are determined within the reaction volume.

(ii) The second step concerns the $5d_{3/2}7h[K]$ $J=5\rightarrow 4f_{5/2}7h$ $J'=4-6$ excitation processes with $K=11/2$ and 9/2. The $5d7h$ wave functions extend too far out to permit a correct description of $5d7h$ levels within the reaction volume of radius $r_0=50$ a.u. and excitation spectra are calculated using the ICE approximation.

The validity of this approximation relies mainly on the absence of spatial overlap between the inner and outer elec-

tron orbitals. We have checked that this nonoverlapping property holds in both initial and final states. Our excitation scheme is comparable to the excitation of the $4f5g$ from $5f5g$ levels [11]. It was recently shown that the ICE approximation well describes the excitation of the $4f5g$ levels, although these levels are the lowest members of the $4fng$ Rydberg series [30].

The initial states are of the type $\Psi_0=\Phi_0 P_0(\nu_0,r)$, where Φ_0 denotes the $5d_{3/2}n'h[K]$ $J=5$ channel function; ν_0 is the effective quantum number.

The ICE approximation is based on negligible continuum excitation and excitation of the inner electron only. The wave function of the initial state of the Rydberg electron is projected on that of the excited state.

The transition moment for the closed channel i is given by

$$D_i=\langle\Phi_0|D|\Phi_i\rangle\langle P_0(\nu_0,r)|P_i(\nu_i,r)\rangle, \tag{3}$$

where the one-photon transition moment implicitly contains all the angular coefficients related to the polarizations of the two lasers involved in the excitation process as well as those related to the decoupling of the individual angular momenta and spins from the total angular momentum. In Eq. (3), the overlap integral for the outer electron $\langle P_0(\nu_0,r)|P_i(\nu_i,r)\rangle$ is approximately proportional to $\delta(l_0,l_i)\sin\pi(\nu_i-\nu_0)/(\nu_i-\nu_0)$. l_0 and l_i are the orbital momenta of the outer electron in the initial and final state [33]. Starting from a pure jK-coupled $5d_{3/2}7h[K]$ level, because of the $\delta(l_0,l_i)$ function, only the transition moments D_i associated with $4f_{5/2}7h$ channels have nonzero values, i.e., only these latter channels are excited directly. The influence of deviations from pure jK coupling for the $5d_{3/2}7h$ levels will be discussed in Sec. IV.

The partial photoionization cross section in the open channel i' is given by

$$\sigma_{i'}=4\pi^2\alpha\omega\left|\sum_{\rho}\sum_{i\in c}T_{i'\rho}Z_{i\rho}D_i\exp(i\pi\tau_\rho)\right|^2, \tag{4}$$

where α is the fine-structure constant and ω the photon frequency [34].

The calculation of partial photoionization cross sections corresponding to the decay into the various continua allows for the computation of theoretical spectra comparable to the experimental spectra as well as for the analysis of the autoionization mechanisms of final states.

3. Phase-shifted MQDT parameters

The phase-shifted MQDT formulation [20,27,28] is used in this paper to analyze the interfering resonance patterns observed in the excitation spectra of $4f_{5/2}7h$ levels from $5d_{3/2}7h$ levels. This analysis is performed in two steps. First, from the complete short-range reaction matrix obtained with the R-matrix method energy-dependent phase-shifted MQDT parameters describing the interactions between the N_c closed channels and the N_0 continua relevant to the energy range under study are calculated for each J' value. This is done by using the formulation worked out by Lecomte [28]. Then a simplified phase-shifted MQDT model deduced from the complete phase-shifted treatment is used to analyze the interference pattern observed in excitation from the $5d_{3/2}7h[11/2]$ $J=5$ level. The procedure used to determine the complete sets of phase-shifted parameters is briefly outlined here, while the simplified treatment using a three-channel MQDT model will be presented later in Sec. IV.

In phase-shifted MQDT, the general problem of N interacting channels ($N=N_0+N_c$) is reduced to a simpler problem involving closed channels only, the presence of open channels being taken into account globally. Restricting the reaction matrix $K(E)$ to the closed-channel set and defining fragmentation channels on phase-shifted Coulomb functions, phase-shifted quantum defects μ_i and a transformed complex reaction matrix κ'_{cc} are obtained with elements of the form

$$\kappa'_{ij}=r_{ij}+i\mathbf{R}_i\cdot\mathbf{R}_j, \tag{5}$$

with $r_{ii}=0$. As detailed elsewhere [28], the real r_{ij} elements describe the direct coupling between the closed channels. Moreover, this approach introduces N_c effective continua and the N_c vectors $\mathbf{R}_i$, involved in the imaginary part of the κ' matrix, describe the couplings between the closed channels and the effective continua. When the resonances pertaining to channel i are well separated from the others, μ_i and $|\mathbf{R}_i|^2$ characterize the positions and scaled autoionizing widths $\gamma_i=\Gamma_i(\nu_i)^3=2|\mathbf{R}_i|^2/\pi$ (Γ_i is the FWHM autoionization width in a.u.) of the resonances in channel i. In addition, the evaluation of the effective continua in terms of the jj-coupled open fragmentation channels permits the branching ratios for autoionization to be calculated for each closed channel, i.e., to analyze the continua to which autoionizing levels preferentially decay.

IV. RESULTS AND DISCUSSION

A. Intermediate $5d_{3/2}7h$ levels

The $5dnh$ configurations all lie above the first ionization limit at 42 034.90 cm^{-1} and autoionize into $6s_{1/2}\epsilon l$ continua. The autoionization rates are low; for the $5d_{5/2}nh$ $J=5$ states above the $5d_{3/2}$ threshold ($n=20$–50) a scaled autoionization rate $n^3\Gamma=800$ GHz (FWHM) was reported [35]. The $5dnh$ states can be excited from $5d^2$ states due to configuration interaction between $5dnf$ and $5dnh$ states. In the experiment we only observed $5dnh$ states in the vicinity of $5dnf$ resonances. An example is given in Fig. 2, where the spectrum of the laser excitation from the metastable $5d^2\,{}^1G_4$ state at 24 696.28 cm^{-1} is shown. The $5d_jnh[K]$ $J=5$ levels with $n=6$ and 7 interact with the strong $5d_{3/2}6f$ $J=5$ resonance at 44 652.85 cm^{-1} [35], resulting in asymmetric line profiles. The spectrum in Fig. 2, taken at low laser power (10 μJ/pulse), shows the $5d_{3/2}7h[11/2]$ $J=5$ state. At higher laser power the $5d_{3/2}7h[9/2]$ $J=5$ is observed as well. Both states were also excited from the $5d^2\,{}^3F_4$ metastable state at 21 623.75 cm^{-1}. The observed linewidths for the $5d_{3/2}7h$ $J=5$ states are close to laser linewidth (0.067 cm^{-1}). The $5d_3/27h[7/2]$ state was excited from the $5d^2\,{}^3F_3$ metastable state at 21 250.17 cm^{-1}. We also observed $5d_{3/2}14h$ $J=5$ and $5d_{5/2}9h$ $J=5$ states located near the $5d_{3/2}14f_{7/2}$ $J=5$ state in excitation from the $5d^2P\,{}^1G_4$ state. Using high laser powers of 10 mJ/pulse, some other $5dnh$ states could be excited from the $5d^2\,{}^1G_4$ state. The energy positions of the observed $5dnh$ states are collected in Table I. The

TABLE I. Energy positions (in cm^{-1}) of the observed $5d_j nh$ states with respect to $6s^2\ ^1S_0$ ground state; uncertainties 0.15 cm^{-1}.

Level / K	11/2	9/2	7/2
$5d_{3/2}6h$	43 848.09	43 851.18	
$5d_{3/2}7h$	44 661.16	44 663.16	44 670.01
$5d_{3/2}11h$	45 999.66		
$5d_{3/2}14h$	46 347.77	46 347.96	
$5d_{5/2}6h$	44 648.25	44 651.54	
$5d_{5/2}9h$	46 350.85	46 351.87	

$5d_{3/2}7h[11/2]5$ and $5d_{3/2}7h[9/2]5$ levels were used as intermediates in the two-step excitation of $4f_{5/2}7hJ'$ levels from $5d^2\ ^1G_4$ and $^3F_4$ levels, respectively.

R-matrix calculations for the odd-parity $J=4$ and 5 symmetries below the $5d_{3/2}$ limit give energy positions of $5dnh$ levels and the mixing of $5dnh$ levels with $5dnf$ levels. As explained elsewhere [28,31] the complete reaction matrix $K(E)$ referring to closed and open channels for a given J value can be contracted to give an effective reaction matrix restricted to closed channels only. Using this matrix, MQDT techniques adapted to bound spectra can be used to calculate the energy positions of resonant levels, to identify the levels, and to display channel mixing by drawing Lu-Fano plots. The Lu-Fano plots obtained in this way for $J=4$ and 5 are very similar those obtained empirically by Bente and Hogervorst [35,36] from the energy positions of $5dnf$ levels. However, the theoretical Lu-Fano plots account in addition for the mixing of $5dnf$ Rydberg series with $5dnh$ and $5dnp$ (for $J=4$) series. Theoretical energy positions for $5dnf$ and $5dnh$ levels agree well with the measured energies, deviations being for most of the levels smaller than 1 cm^{-1}. The $5dnh$-$5dnf$ mixing is extremely small except when the $5dnh$ and $5dnf$ levels are very close in energy. The quantum defects of $5dnh$ series have values of the order of 0.01–0.02. Due to their interaction with $5d_{5/2}nf$ levels some $5d_{3/2}nf$ levels are shifted toward similar small quantum defects. This occurs for the $5d_{3/2}7f$ and $5d_{3/2}14f$ $J=5$ levels. This fully supports the fact that at low laser powers only $5dnh$ $J=5$ levels in the vicinity of the $5d_{3/2}7f$ and $5d_{3/2}14f$ $J=5$ levels have been observed in excitation from $5d^2$ levels. It must be noted that for $n\leqslant 20$, the quantum defects of $5d_{3/2}nf$ $J=4$ levels are $\geqslant 0.08$, even for levels close to the $5d_{5/2}nf$ levels.

We also calculated the excitation spectra of $J=4$ and 5 levels form the $5d^2\ ^1G_4$ and $^3F_4$ levels in the 44 654–44 670-cm^{-1} energy range displayed in Fig. 2. The excitation spectra of $J=5$ levels show five peaks associated with the $5d_{5/2}6h$ ($K=11/2$ and 9/2), $5d_{3/2}7f_{7/2}$ and $5d_{3/2}7h$ ($K=11/2$ and 9/2) levels while the excitation spectra of $J=4$ levels show four peaks associated with the $5d_{5/2}6h$ and $5d_{3/2}7h$ ($K=9/2$ and 7/2) levels. Because the $5d_{3/2}7f_{5/2}$ and $5d_{3/2}7f_{7/2}$ $J=4$ levels, at 44 602.2 and 44 614.8 cm^{-1}, respectively [35], are far from the $5dnh$ levels, the excitation cross sections of $J=4$ levels are several orders of magnitude smaller than those of $J=5$ levels. Likewise the $5d_{3/2}7f_{5/2}$ and $5d_{3/2}7f_{7/2}$ $J=3$ levels lie [37] far from the expected positions of $5d_{5/2}6h$ and $5d_{3/2}7h$ $J=3$ levels. In conclusion, the $5dnh$ levels observed from the $5d^2$ $J=4$ levels can be assigned to have $J=5$.

To conclude this analysis we give some additional information on the wave functions of the $5d_{3/2}7h[K]$ $J=5$ levels with $K=11/2$ and 9/2. The $5d_{3/2}7h[11/2]$ level is extremely pure (~99%), the weights of $5d_j7f_{j'}$ components in the wave function expansion being smaller than 0.2%. The $5d_{3/2}7h[9/2]$ level is slightly mixed with the $5d_{5/2}6h[9/2]$ level (3%) but the $5d_j7f_{j'}$ components are again small ($\leqslant 0.8\%$).

B. Complex resonances associated with $4f_{5/2}7h$ levels

1. Contribution of 4f7f levels

As discussed in Sec. IV A, the $5d_{3/2}7h[K]$ $J=5$ levels with $K=9/2$ and 11/2 are weakly mixed with $5d7f$ levels. Two $4f7f$ levels are predicted [8,24] to be located between the $6d_{3/2}$ and $6d_{5/2}$ thresholds, so we first checked whether the observed structures may be associated with these levels. The $4f7f\ ^3H_6$ level is expected at 88 010 cm^{-1} with an unperturbed width (see Sec. III B 1) of 50 cm^{-1}, while the $4f7f\ ^3F_4$ level at 88 095 cm^{-1} has an unperturbed width of 40 cm^{-1}. The energy positions and widths obtained in the present work agree with those of Ref. [26]. However, we found that these levels are better described in jj than in LS coupling, both corresponding to $4f_{7/2}7f_{7/2}$ levels. We have calculated the ICE excitation spectra of these $J'=4$ and 6 levels from $5d_{3/2}7h[9/2]$ $J=5$ by considering in the wave function of the initial state only the small $5d_{5/2}7f$ components ($\leqslant 0.3\%$) from which the $4f_{7/2}7f_{7/2}$ levels may be excited. The excitation spectra exhibit complex resonances around the position of the $4f_{7/2}7f_{7/2}$ $J'=4$ and 6 levels but the cross sections are two to three orders of magnitude smaller than those obtained by assuming the $5d_{3/2}7h[9/2]$ $J=5$ level is not mixed with $5d_j7f_{j'}$. Thus the observed structures correspond undoubtedly to $4f_{5/2}7h$ levels. We have also checked that the other small components in the wave-function expansion of the $5d_{3/2}7h[K]$ $J=5$ initial levels do not contribute to the cross sections. Therefore, the results presented below are obtained by assuming that the $5d_{3/2}7h[K]$ $J=5$ initial levels are purely jK coupled.

2. Characteristics of the $4f_{5/2}7h$ levels

The positions, quantum defects and unperturbed widths of the $4f_{5/2}7h[K]J'$ levels obtained by treating the $6d_{5/2}nl'$ channels as open in the MQDT calculations of the $5d_{3/2}7h[K]$ $J=5\rightarrow 4f_{5/2}7h$ $J'=4$–6 spectra with $K=11/2$ and 9/2 are collected in Table II. Due to the negligible contribution of the exchange electrostatic interaction, the two levels $J'=K\pm 1/2$ belonging to the same jK doublet are nearly degenerate and have the same width. In the same table, the continua which contribute significantly to the autoionization branching ratios of $4f_{5/2}7h[K]$ levels are listed. These results, obtained using phase-shifted MQDT parameters, agree with those derived from the R-matrix calculations for the partial photoionization cross sections of the $5d_{3/2}7h[K]$ $J=5\rightarrow 4f_{5/2}7h$ $J'=4$–6 processes. The $4f_{5/2}7h[K]$ states are found to decay primarily into the $6d_{3/2}\epsilon i$ or $6d_{3/2}\epsilon g$ continua (dipole-induced autoionization). Levels decaying preferentially to the $6d_{3/2}\epsilon g$ continua have

TABLE II. Characteristic parameters of $4f_{5/2}7h[K]J'$ states derived from R-matrix calculations. Energy positions relative to the $6s^2\ ^1S_0$ ground state, quantum defects with respect to the $4f_{5/2}$ threshold, "unperturbed widths" (see Sec. III), branching ratios for autoionization, and dipole matrix elements in excitation from $5d_{3/2}7h[11/2]5$ and $5d_{3/2}7h[9/2]5$ are given.

State	E (cm^{-1})	μ	Γ (cm^{-1})	Branching ratios (%)	d_i [a]	d_i [b]
$4f_{5/2}7h[11/2]5$	88 029.4	+0.038	27	$6d_{3/2}\epsilon i(85)$	−1.513	−0.182
$4f_{5/2}7h[11/2]6$	88 031.4	+0.035	28	$6d_{3/2}\epsilon i(85)$	+0.134	−1.047
$4f_{5/2}7h[13/2]6$	88 035.7	+0.029	99	$6d_{3/2}\epsilon i(99)$	−1.346	0.0
$4f_{5/2}7h[9/2]4$	88 043.5	+0.016	6.0	$6d_{3/2}\epsilon g(77),7s\epsilon g(9)$	−0.551	−0.147
$4f_{5/2}7h[9/2]5$	88 043.5	+0.016	5.9	$6d_{3/2}\epsilon g(64),6d_{3/2}\epsilon i(23)$	+0.114	−1.650
$4f_{5/2}7h[7/2]4$	88 073.6	−0.038	5.9	$6d_{3/2}\epsilon g(41),7s\epsilon g(27),6p_j\epsilon l'(16)$	0.0	−0.841

[a]Initial level: $5d_{3/2}7h[11/2]5$.
[b]Initial level: $5d_{3/2}7h[9/2]5$.

smaller autoionization widths ($\Gamma\sim 6$ cm^{-1}) than those ($\Gamma\geqslant 27$ cm^{-1}) decaying mainly to the $6d_{3/2}\epsilon i$ continua. The differences in the widths of $4f_{5/2}7h[K]$ levels with $K=11/2$ and 13/2 are related to the differences in angular factors involved in the dipolar coupling terms. Octupole autoionization to $7s\epsilon l'$ continua is weak ($\leqslant 9\%$) except for the $4f_{5/2}7h[7/2]$ $J'=4$ level which decays significantly (27%) into the $7s\epsilon g$ continua. This state is the only level for which decay into continua built on a low-lying Ba^+ core is not negligible. Here the branching ratio associated with $6p\epsilon l'$ continua amounts to 16%.

The relative values d_i of the angular parts of the dipole matrix elements D_i associated with the excitation of purely jK-coupled $4f_{5/2}7h[K]$ $J'=4-6$ levels from the purely jK-coupled $5d_{3/2}7h[11/2]$ and $5d_{3/2}7h[9/2]$ $J=5$ levels are also collected in Table II. The d_i values strongly depend on the initial state. From the $5d_{3/2}7h[11/2]$ $J=5$ level, $4f_{5/2}7h[K]$ J' levels with $J'=K-1/2$ are predominantly excited while from the $5d_{3/2}7h[9/2]$ $J=5$ level the excitation of $4f_{5/2}7h[K]$ J' levels with $J'=K+1/2$ is favored.

3. $4f_{5/2}7h$ excitation spectra

Excitation spectra were recorded, detecting Ba^{2+} ions produced by photoionization of Ba^+ $6d_{3/2}$ and $7s$ ions with the UV photons also used to excite $4f_{5/2}7h$ levels from $5d_{3/2}7h$ levels. The photoionization cross sections of the Ba^+ ions at the energy of the UV photons were obtained by a calculation in a central potential model approximation [38]. Due to the prevalence of the $6d\rightarrow\epsilon f$ transition over the $7s\rightarrow\epsilon p$ transition, photoionization of $6d_{3/2}$ ions is found to be 30 times more probable than that of $7s$ ions.

As photoionization of $7s$ ions is weak, experimental spectra are compared with the partial photoionization cross sections of the $5d_{3/2}7h[K]$ $J=5\rightarrow 4f_{5/2}7h$ J' processes (summed for $J'=4-6$) corresponding to electron ejection into the $6d_{3/2}\epsilon l'$ continua only. The comparison between experiment and theory is shown in Figs. 3 and 4. The theoretical spectra in Figs. 3(b) and 4(b) have been convoluted with an instrumental linewidth of 0.2 cm^{-1}.

The spectrum of Fig. 3 displays a complex pattern of interfering resonances. All resonances fall within the central lobe of the overlap integral of Eq. (3) which is maximum at 88 046 cm^{-1} ($5d_{3/2}\rightarrow 4f_{5/2}$ ionic transition). Clearly, in addition to $4f_{5/2}7h$ $J=4-6$ resonances, which are directly accessible in the ICE process, resonances pertaining to autoionizing Rydberg series converging to the Ba^+ $6d_{5/2}$ threshold show up in the spectra. The identification of the intense and narrow peaks on both sides of the central broad features is deduced from the phase-shifted MQDT r_{cc} parameters [Eq. (5)], which describe the direct coupling between closed channels and from the analysis of the energy dependence of the density of states [Eq. (4)] in each closed channel. For each J' value the matrix elements r_{cc} associated with $4f_{5/2}nh-6d_{5/2}ni$ mixing are 3–10 times larger than the largest elements for the interaction of $4f_{5/2}nh$ and $6d_{5/2}nd$, $6d_{5/2}ng$, or $6d_{5/2}nk$ channels. The strong $4f_{5/2}nh-6d_{5/2}ni$ mixing is reflected in the energy dependences of the density of states in $6d_{5/2}ni$ and $4f_{5/2}nh$ channels. In the absence of perturbations the $6d_{5/2}ni$ density-of-state profiles should display a regular pattern of narrow peaks with constant intensity. In fact the $4f_{5/2}7h$ perturbers induce an irregular variation of their positions, widths, and intensities. The $4f_{5/2}nh$ density-of-states profiles associated with $4f_{5/2}nh$ closed channels exhibit complex resonance patterns similar to those visible in Fig. 3, differences between density of states profiles and ICE spectra resulting from the dipole matrix elements. We conclude that the intense and narrow peaks on both sides of the central broad features in Fig. 3 can be identified with the $6d_{5/2}ni$ Rydberg levels with $23\leqslant n\leqslant 37$.

Figure 3(c) shows the relative contribution of each final J' value to the theoretical spectrum. From this figure as well as from the energy positions of the $4f_{5/2}7h[K]J'$ levels and the d_i values given in Table II an assignment of all the resonances in Fig. 3(b) follows.

The broad resonance at 88 031 cm^{-1} corresponds to the $4f_{5/2}7h[11/2]$ $J'=5$ level, the narrow peak at 88 037 cm^{-1} to the $6d_{5/2}27i$ $J'=4$ level, and the two-peak structure at 88 039–88 043 cm^{-1}, partially masked by the ion signal in Fig. 3(a), to the $6d_{5/2}27i$ $J'=5$ and $4f_{5/2}7h[9/2]$ $J'=4$ levels. These intense resonances are superimposed on the very broad $4f_{5/2}7h[13/2]$ $J'=6$ resonance. Although the d_i value associated with this resonance is large, the cross section is relatively small as it is proportional to $(d_i)^2/\Gamma$ and the unperturbed width Γ is large (99 cm^{-1}).

The $6d_{5/2}ni$ levels with $n\leqslant 26$ lying on the low-energy side of the broad $4f_{5/2}7h$ $J=4-6$ resonances are characterized by negative values of the line-shape parameter q [25]. The $6d_{5/2}ni$ levels with $n\geqslant 28$, on the right side of the broad

central structures, have positive values of q. The width of $6d_{5/2}ni$ levels strongly depends on n. The $6d_{5/2}23i$ level, located below the $6d_{3/2}$ ionization limit, as well as the $6d_{5/2}24i$ level are extremely narrow. The predicted widths for these levels, respectively, are 0.08 and 0.15 cm^{-1}, which are below the instrumental linewidth of 0.2 cm^{-1}. These widths correspond to the overlapping features of $J=4-6$ symmetries and, in fact, for the $J'=5$ resonances, widths ≤ 0.01 cm^{-1} are predicted. As follows from Fig. 3(c) the $6d_{5/2}ni$ levels correspond predominantly to $J'=5$ and 6 and, for a given J' value, both K components are degenerate. The $6d_{5/2}ni$ levels, which cannot be excited directly from the $5d_{3/2}7h[11/2]$ $J=5$ level, show up in the ICE spectrum due to their mixing with the $4f_{5/2}7h$ levels. In contrast, the $6d_{5/2}nd$ $J=4,5$, $6d_{5/2}ng$ $J=4-6$, and $6d_{5/2}nk$ $J=5,6$ autoionizing Rydberg series, which have small or negligible mixing with the $4f_{5/2}7h$ levels, do not appear in the spectrum.

Despite the complexity of the problem involving three final J' spectra, each requiring a correct description of the interactions between a large number of channels, the agreement between the experimental and theoretical spectra in Fig. 3 is excellent. Clearly, the R-matrix approach successfully reproduces the complicated interference pattern involving q reversal and stabilization against autoionization in the $6d_{5/2}ni$ series interacting with the $4f_{5/2}7h$ levels. The positions and profiles of all resonances are well reproduced. A more detailed analysis of the interference and q-reversal effects will be presented later in Sec. IV C.

Figure 4 shows the excitation spectrum starting from the $5d_{3/2}7h[9/2]$ $J=5$ level, which also exhibits a complicated pattern of interfering resonances. It is again due to the interaction of the $4f_{5/2}7h$ levels with mainly the $6d_{5/2}ni$ series. From the $5d_{3/2}7h[9/2]$ $J=5$ level, as follows from the last column of Table II, three $4f_{5/2}7h[K]J'$ levels have large excitation dipole matrix elements $d_{\tilde{i}}$. The broad structure at 88 032 cm^{-1} mainly corresponds to the $4f_{5/2}7h[11/2]$ $J'=6$ level on which the sharp and narrow $6d_{5/2}27i$ $J'=5$ resonance is superimposed. The $4f_{5/2}7h[9/2]$ $J'=5$ level is associated with the central intense peak, hidden in Fig. 4(a) under the ionic signal. The structured resonance around 88 075 cm^{-1} corresponds to the $4f_{5/2}6h[7/2]$ $J'=4$ level interfering with neighboring $6d_{5/2}nl'$ $J'=4$ levels, mainly with $L'=6$. As in Fig. 3, the interactions of the $4f_{5/2}7h$ levels with the $6d_{5/2}ni$ series result in a q reversal along the $6d_{5/2}ni$ series. Here again the agreement between the experimental and theoretical spectra is excellent, except in the energy range 88 070–88 090 cm^{-1}, where the $4f_{5/2}7h[7/2]$ $J'=4$ level is located. The calculated position of this level is shifted compared to the experiment to lower energy by ~ 10 cm^{-1}, corresponding to only a small change in the quantum defect of 0.015.

A remarkable feature observed both in excitation from $5d_{3/2}7h$ $K=9/2$ and 11/2 levels is the intensity of the $6d_{5/2}23i$ resonance. This state is located just below the $6d_{3/2}$ ionization limit where it interacts with high-n members of $6d_{3/2}nl'$ Rydberg series. The $6d_{5/2}23i$ state can only be observed if it autoionizes into the $7s$ continuum. The calculation of the intensity of the $6d_{5/2}23i$ resonance leads to numerical problems since the $6d_{3/2}ni$ series just below the $6d_{3/2}$ threshold are so dense and narrow. Therefore we treated the $6d_{5/2}23i$ level as if it decays into the $6d_{3/2}$ continuum as well. Because of this assumption the theoretical spectra are below the $6d_{3/2}$ threshold shown as a dashed line. The remarkable feature is that, despite the much smaller photoionization cross section of $7s$ ions compared to $6d$ ions, the experimental intensity of the $n=23$ resonance is only slightly lower than that of the $n=24$ level located above the $6d_{3/2}$ threshold. A detailed treatment of the $6d_{5/2}ni$ series below the $6d_{3/2}$ threshold is required to come to a complete understanding of the intensity of the $6d_{5/2}23i$ resonance, but this falls outside the scope of this work.

C. Three-channel MQDT analysis

From Fig. 3(c) it follows that the final $J'=5$ value predominantly contributes to the complex interference pattern and q reversal also shown in Fig. 3(b). Above the Ba^+ $6d_{3/2}$ threshold, the $J'=5$ spectrum involves 20 closed channels interacting with 24 open channels. This situation is much more complicated than in the cases studied in Refs. [18,19], which involve the two $5d_{3/2}nd_{3/2}$ and $5d_{5/2}nd_{5/2}$ $J=0$ autoionizing Rydberg series in Ba coupled to the $6s\epsilon s$ $^1S_0$ continuum. Examination of the phase-shifted MQDT parameters deduced from R-matrix calculations shows that for $J'=5$, to a good approximation, the 44-channel problem can be reduced to a three-channel problem. In fact, above the $6d_{3/2}$ ionization threshold the $4f_{5/2}7h[11/2]$ $J'=5$ level, which is the only strongly excited level, is mainly coupled to the $6d_{5/2}ni[11/2]$ Rydberg series, and both the $4f7h$ level and the $6dni$ Rydberg levels mainly decay into the same $6d_{3/2}\epsilon i[11/2]$ continuum.

We performed a three-channel MQDT treatment of the $J'=5$ spectrum (above the $6d_{3/2}$ limit) using a set of five phase-shifted parameters whose values are fixed at the values obtained from the complete treatment. In contrast to previous analysis of complex resonances [17–19] using phase-shifted MQDT parameters fitted to experimental data, in the present treatment the parameters are calculated using the R-matrix approach. Denoting by (1) the continuum and by (2) and (3) the channels converging to the $6d_{5/2}$ and $4f_{5/2}$ thresholds, respectively, the parameters are the quantum defects $\mu_2=0.1522$ and $\mu_3=0.0330$ associated with the closed channels, $r_{23}=-0.1400$ for the coupling between the closed channels and $r_{12}=0.1004$ and $r_{13}=0.2026$ for the coupling of the closed channels with the continuum. Note that the two latter parameters correspond to the lengths of the vectors $\mathbf{R}_i$ introduced in Eq. (5). Calculation of the photoionization cross sections requires three additional transition dipole moment parameters D_i. Since only the $4f_{5/2}nh$ channel is excited in the ICE process $D_1=D_2=0$. This implies that the interference pattern does not result from interferences in the excitation process but from interferences in the autoionization due to the mixing of closed channels. More precisely, the interference effects can be analyzed in terms of those occurring in the density of states or channel weight $(Z_3)^2$ in the $4fnh$ channel (3). Indeed, the photoionization cross section [21] is proportional to $(Z_3)^2$:

$$\sigma=\frac{(Z_3)^2(D_3)^2}{1+(T_3)^2}, \tag{6}$$

with the abbreviated notation $T_i=\tan\pi(\nu_i+\mu_i)$ $(i=2,3)$.

For $(Z_3)^2$, Cooke and Cromer [20] derived the following expression:

$$(Z_3)^2=(r_{13})^2\frac{1+(T_3)^2}{(T_3)^2+(r_{13})^4}\frac{(T_2-s_2+q_2b_2)^2}{(T_2-s_2)^2+(b_2)^2}. \quad (7)$$

In (7), $(Z_3)^2$ is expressed in terms of the rapidly changing variable T_2. The first factor of Eq. (7) corresponds to the profile of the broad resonance in channel (3) in the absence of interaction between both series $(i=2,3)$. The second factor is a rapid modulation, for each cycle of ν_2, describing a sequence of Fano-like profiles caused by the interaction between channels (2) and (3). The quantities s_2, b_2, and q_2 correspond to shifts in resonance energy, widths, and line-shape parameter given by

$$s_2=\frac{T_3[(r_{23})^2-(r_{12})^2(r_{13})^2]+2r_{12}r_{23}(r_{13})^3}{(T_3)^2+(r_{13})^4}, \quad (8)$$

$$b_2=\frac{(r_{12}T_3-r_{23}r_{13})^2}{(T_3)^2+(r_{13})^4}, \quad (9)$$

$$q_2=-\frac{T_3r_{23}+(r_{13})^3r_{12}}{r_{13}(T_3r_{12}-r_{13}r_{23})}. \quad (10)$$

These parameters are functions of the slowly changing variable T_3.

Results obtained with this simplified three-channel MQDT model are shown in Fig. 5. In Fig. 5(a) the energy variation of $(Z_3)^2$ is compared to the cross section of $5d_{3/2}7h[11/2]$ $J=5\rightarrow 4f_{5/2}7h$ $J'=5$ ICE spectrum obtained with the complete treatment involving 44 interacting channels. Note that the $[Z_3(E)]^2$ profile has been convoluted with the instrumental linewidth and renormalized to give the same height at the central broad peak. Except for slight shifts of the resonances in the middle of the figure, both curves of Fig. 5 agree well, justifying the use of the three-channel MQDT model to analyze interference effects in the $J'=5$ spectrum. The q_2 and b_2 parameters are plotted in Figs. 5(b) and 5(c) against energy. The zero value of q_2 at 88 034 cm^{-1} occurs close to the center of the $4f_{5/2}7h$ resonance and explains the symmetric shape of this resonance. The variation in the width parameters b_2 well reproduces the evolution observed experimentally. Vanishing width should occur at the energy for which $|q_2|$ has an infinite value and b_2 a zero value. As visible in Figs. 5(b) and 5(c) at the $6d_{3/2}$ ionization threshold, the value of $|q_2|$ is large and the value of b_2 very small and, in fact, the point of vanishing width predicted by this three-channel MQDT model lies just below the threshold. This agrees with the observation of an extremely narrow width for the $6d_{5/2}24i$ level. The variation of q_2 well reproduces the q reversal visible not only in Fig. 5 but also in Fig. 3 which involves the sum of the spectra with three final J' values.

It must be emphasized that the line-shape parameter q_2 used to analyze the q reversal along the $6d_{5/2}ni$ autoionizing Rydberg series differs from the Fano q parameter [25], which is proportional to the ratio of the transition amplitude to the resonant state and the amplitude of direct photoionization. Here the interference effect occurs in the spectral density of autoionizing states and not in the excitation. The dramatic changes of the widths and the q reversal along the $6d_{5/2}ni$ autoionizing Rydberg series result from interference between direct autoionization and indirect autoionization via the $4f_{5/2}7h$ broad interlopers of the Rydberg series.

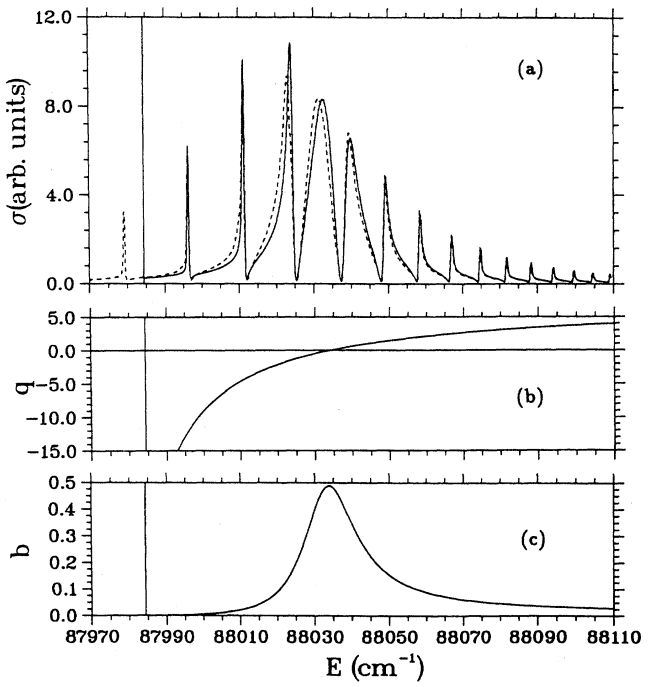

FIG. 5. Results from a three-channel MQDT model. (a) Comparison between the energy variation of the $4f7h$ perturber weight $(Z_3)^2$ defined in Eq. (7) (full line) and the $5d_{3/2}7h[11/2]$ $J=5\rightarrow 4f_{5/2}7h$ $J'=5$ cross section from the complete 44-channel treatment (dashed line). (b) Energy dependence of the $|q_2|$ parameter related to the line shape of the $6d_{5/2}ni$ resonances. (c) Energy dependence of the b_2 parameter corresponding to the width of the $6d_{5/2}ni$ levels. Stabilization against autoionization occurs at the energy for which b_2 has zero value and q_2 is infinite. The energy at which this occurs lies below the $6d_{3/2}$ threshold at 87 984 cm^{-1}, where the simple three-channel model is not valid.

The interference pattern occurring in the $5d_{3/2}7h[9/2]$ $J=5\rightarrow 4f_{5/2}7h$ $J'=4-6$ spectrum cannot be analyzed with a similar three-channel MQDT model, mainly because all final J' values contribute significantly. However, here again, the interference effects occur in the spectral density of autoionizing states and not in the excitation process.

V. CONCLUSION

The autoionizing $4f_{5/2}7h$ $J'=4-6$ levels of Ba interacting with $6d_{5/2}ni$ Rydberg series have been studied, both experimentally and theoretically. The excitation spectra of doubly excited $4f7h$ states show complex interference patterns which are reproduced in eigenchannel R-matrix calculations in combination with MQDT. In these calculations almost all channels (≈ 40) were taken into account for each symmetry, while the radius of the reaction volume was taken at 50 a.u. The agreement between experiment and theory is excellent for excitation via the $5d_{3/2}7h$ $K=11/2$ intermediate state and

satisfactory for excitation via the $K=9/2$ intermediate level. In both cases the observed features such as q reversal along the $6dni$ series and stabilization against autoionization of the $6dni$ levels are reproduced.

The interference pattern for $J=5$ is also analyzed in terms of a three-channel phase-shifted R-matrix model. It is shown that the interferences occur in the spectral density of states and do not result from the laser excitation. Experimentally the widths of $6d_{5/2}23i$ and $6d_{5/2}24i$ are determined by the instrumental width of 0.2 cm^{-1}. In the calculations for the $J=5$ symmetry a width narrower than 0.01 cm^{-1} is predicted, corresponding to a lifetime of more than 0.5 ns. This phenomenon of stabilization is remarkable in view of the high excitation energy of the states.

Because the $6dni$ levels are rather long lived, these levels could be used as intermediate levels for further excitation to double-Rydberg states with a high l for both electrons in an experiment with nanosecond pulsed lasers. The composition of the wave functions determined from the present R-matrix calculations could be used to identify the states ultimately excited.

ACKNOWLEDGMENTS

Numerical calculations were carried out on the Cray 98 computer belonging to the "Institut du Développement et des Ressources en Informatique Scientifique" of the Centre National de la Recherche Scientifique and on the Cray YMPEL of the computer center "Paris Sud Informatique."

[1] R. R. Jones and T. F. Gallagher, Phys. Rev. A **42**, 2655 (1990).
[2] P. Camus, T. F. Gallagher, J. M. Lecomte, P. Pillet, and L. Pruvost, Phys. Rev. Lett. **62**, 2365 (1989).
[3] U. Eichmann, V. Lange, and W. Sandner, Phys. Rev. Lett. **64**, 274 (1990).
[4] C. H. Greene and L. Kim, Phys. Rev. A **36**, 2706 (1987).
[5] M. Aymar, J. Phys. B **23**, 2697 (1990).
[6] C. H. Greene and M. Aymar, Phys. Rev. A **44**, 1773 (1991).
[7] R. P. Wood and C. H. Greene, Phys. Rev. A **49**, 1029 (1994).
[8] M. Aymar, E. Luc-Koenig, and J. M. Lecomte, J. Phys. B **27**, 2425 (1994).
[9] E. Luc-Koenig, J. M. Lecomte, and M. Aymar, J. Phys. B **27**, 699 (1994).
[10] R. J. de Graaff, W. Ubachs, and W. Hogervorst, Phys. Rev. A **45**, 166 (1992).
[11] R. R. Jones, Panming Fu, and T. F. Gallagher, Phys. Rev. A **44**, 4620 (1991).
[12] W. E. Cooke, T. F. Gallagher, S. A. Edelstein, and R. M. Hill, Phys. Rev. Lett. **40**, 178 (1978).
[13] U. Eichmann, V. Lange, and W. Sandner, Phys. Rev. Lett. **68**, 21 (1992).
[14] P. Camus, S. Cohen, L. Pruvost, and A. Bolovinos, Phys. Rev. A **48**, R9 (1993).
[15] W. E. Cooke and T. F. Gallagher, Phys. Rev. Lett. **41**, 1648 (1978).
[16] J. P. Connerade and M. W. D. Mansfield, Proc. R. Soc. London Ser. A **346**, 565 (1975).
[17] J. P. Connerade, J. Phys. B **15**, L881 (1982).
[18] M. Aymar, J. Phys. B **18**, L763 (1985).
[19] J. Neukammer, H. Rinneberg, G. Jönsson, W. E. Cooke, H. Hieronymus, H. König, K. Vietzke, and H. Springer Bolk, Phys. Rev. Lett. **55**, 1979 (1985); H. Hieronymus, J. Neukammer, and H. Rinneberg, J. Phys. B **25**, 3463 (1992).
[20] W. E. Cooke and C. L. Cromer, Phys. Rev. A **32**, 2725 (1985).
[21] A. Giusti-Suzor and H. Lefebvre-Brion, Phys. Rev. A **30**, 3057 (1984).
[22] J. P. Connerade, Proc. R. Soc. London Ser. A **362**, 361 (1978).
[23] A. M. Lane, J. Phys. B **17**, 2213 (1984); J. P. Connerade and A. M. Lane, *ibid.* **18**, L605 (1985).
[24] D. Wintgen and H. Friedrich, Phys. Rev. A **35**, 1628 (1987).
[25] U. Fano, Phys. Rev. **124**, 1866 (1961).
[26] E. Luc-Koenig, M. Aymar, and J. M. Lecomte, Phys. B **27**, 2447 (1994).
[27] A. Giusti-Suzor and U. Fano, J. Phys. B **17**, 215 (1984).
[28] J. M. Lecomte, J. Phys. B **20**, 3645 (1987).
[29] E. Luc-Koenig and M. Aymar, J. Phys. (France) II **2**, 865 (1992).
[30] M. Aymar and E. Luc-Koenig, J. Phys. B **28**, 1211 (1995).
[31] U. Fano and A. R. P. Rau, *Atomic Collisions and Spectra* (Academic, Orlando, 1986).
[32] M. J. Seaton, Rep. Prog. Phys. **46**, 97 (1983).
[33] A. S. Bhatti, C. L. Cromer, and W. L. Cooke, Phys. Rev. A **24**, 161 (1981).
[34] M. Aymar and J. M. Lecomte, J. Phys. B **22**, 223 (1989).
[35] E. A. J. M. Bente and W. Hogervorst, J. Phys. B **22**, 2679 (1989).
[36] E. A. J. M. Bente and W. Hogervorst, Phys. Rev. A **36**, 4081 (1987).
[37] M. C. Baruch, L. Cai, R. R. Jones, and T. F. Gallagher, Phys. Rev. A **45**, 6395 (1992).
[38] M. Aymar, O. Robaux, and S. Wane, J. Phys. B **17**, 993 (1984).